EFFECTS OF COMPRESSIBILITY AND HEAT RELEASE ON ENTRAINMENT PROCESSES IN MIXING LAYERS

Inga Mahle[1], **Joseph Mathew**[2], **Rainer Friedrich**[1]
[1] Fachgebiet Strömungsmechanik, Technische Universität München
Boltzmannstr. 15, D-85748 Garching, Germany
inga.mahle@aer.mw.tum.de
[2] Department of Aerospace Engineering, Indian Institute of Science
Bangalore 560012 India

ABSTRACT

Characteristics of the process of entrainment in plane mixing layers, and the changes with compressibility and heat release, were studied using DNS with simultaneous fluid packet tracking. The Reynolds number is quite high (between 11000 and 37000 based on layer width and velocity difference), and is above the mixing transition. The study confirms recent findings that 1) engulfed fluid volume as well as its growth rate are very small compared with that of the turbulent region and its growth rate, and 2) the process occurs close to the turbulent-nonturbulent boundaries most often. A new finding is that both compressibility and heat release retard the entrainment process so that it takes an O(1) time for vorticity or scalar levels to grow even after growth has been initiated.

INTRODUCTION

Compressible mixing layers do not grow as quickly as incompressible ones. The effect becomes more pronounced as the convective Mach number—a measure of compressibility—increases, as documented clearly by Papamoschou & Roshko (1988). Heat release within the mixing layer also results in a reduced growth rate. Here, we use direct numerical simulations (DNS) to examine changes in the entrainment processes with changes in compressibility and heat release in a search for one or more plausible mechanisms.

Entrainment has often been described as comprising an engulfment of large packets of irrotational fluid from the surrounding non-turbulent region followed by disintegration and acquisition of vorticity well within the turbulent region. Recently, the DNS study of round jets by Mathew & Basu (2002) revealed that the entrainment process may instead, more frequently, be a fast, small-scale process occurring very close to the turbulent-nonturbulent interface. This is termed nibbling and is the earlier view (Corrsin & Kistler, 1955). Subsequently, PIV measurements in a laboratory jet also showed that engulfed fluid volume as well as its growth rate are very small compared with that of the turbulent region and its growth rate, respectively (Westerweel et al., 2005).

A natural question that arises is whether these characteristics observed in round jets are more generally true. The original studies that led to the engulfment view were of plane mixing layers, notably that of Brown & Roshko (1974), and not of round jets. Turbulent plane-mixing-layers exhibit large scale organization into spanwise-coherent rollers. These rollers undergo merging processes, and it is easy to accept that the dominant entrainment mechanism should be engulfment by these rollers. So the plane mixing layer is the configuration that is most likely to show a preference for engulfment over nibbling. In this study, the same kinds of simulations (DNS with fluid particle tracking) and analyses as in Mathew & Basu (2002) have been performed of compressible, plane mixing layers with and without heat release to examine the generality of the entrainment mechanisms. Compressibility and heat release are important when studying entrainment because they both reduce the shear layer growth rate. Changes in compressibility have been imposed by selecting different convective Mach numbers and heat release by including fast chemistry reactions.

Our findings are similar to the previous observations with round jets: engulfed fluid volume and its growth rate are both significantly smaller than the mixing layer volume and its growth rate, respectively; growth of vorticity and concentration in fluid particles, from levels in the freestream to levels in the turbulent region occur close to the turbulent-nonturbulent interfaces. This is strong support that the mechanism of entrainment is generally a small scale process occurring near turbulence boundaries, especially because the Reynolds numbers in our simulations are also much larger (above the mixing transition) than those in the round jet studies. However, entrainment is delayed by compressibility and even more by heat release so that it takes an O(1) time for vorticity or scalar levels to grow even after growth has been initiated (fluid packet has entered the turbulent region).

DNS OF ENTRAINMENT PROCESS IN PLANE MIXING LAYERS

We used a Cartesian coordinate system in which the x-axis is parallel to the mean flow direction, y is the spanwise coordinate over which the flow is statistically uniform, and z is the transverse coordinate as in Fig. 1. The velocity tends to u_1 in the upper stream and $-u_1$ in the lower stream. The convective Mach number $\mathrm{Ma}_c = \Delta u/(c_1 + c_2)$, where the velocity difference between the streams $\Delta u = 2u_1$, and their sonic speeds are c_1 and c_2. The reference length scale for the simulations is the vorticity thickness $\delta_{\omega,0}$ of the initial hyperbolic-tangent velocity profile, and the velocity scale is Δu. Flows at three values of Ma_c (0.15, 0.7, 1.1), with and without reaction (and heat release) are studied. The initial Reynolds number $Re_{\omega,0} = (\rho_o \Delta u \delta_{\omega,0})/\mu_0$ is 640 in all cases. $\rho_0 = (\rho_1 + \rho_2)/2$ and $\mu_0 = (\mu_1 + \mu_2)/2$ are the average density and viscosity, respectively. The upper stream is pure oxygen and the lower stream is pure nitrogen for the inert cases. The density is nearly uniform because the molecular weights are nearly the same. Initially, the temperature and pressure were uniform. Diffusion coefficients were computed

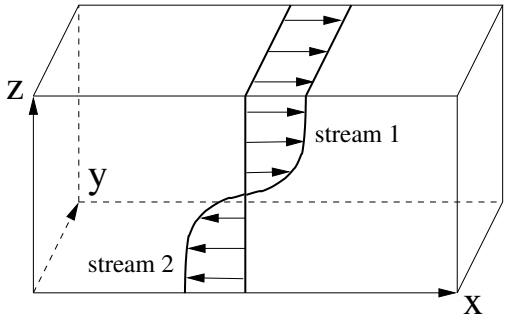

Figure 1: Configuration

Table 1: Simulation parameters. Dimensions of simulated region L_x, L_y and L_z, and numbers of grid points.

	L_x	L_y	L_z	$N_x \times N_y \times N_z$
inert	129.375	32.25	96.75	$768 \times 192 \times 576$
reacting	345	86	172	$768 \times 192 \times 432$

from the local temperature, pressure and species composition; viscosity and heat conductivity from temperature and composition alone. Details are available (Mahle, 2007). For the reacting cases the single step reaction between hydrogen (6.75%) and oxygen (23%) carried in nitrogen streams was taken, with dimensionless heat release rate per unit mass of hydrogen burnt $Q = 7.85$ when scaled with the total enthalpy $c_{p,N_2}T_o$ of the nitrogen stream. Grid and domain sizes are given in Table 1. The simulations with heat release allowed for a coarser resolution due to the smoother flow fields (see below). Temporal simulations were performed with periodicity prescribed in x and y coordinates. The code is based on a pressure-velocity-entropy formulation and has been used for several previous studies (Sesterhenn, 2001, Mahle, 2007). Pathlines of many fluid particles were computed simultaneously as in Mathew & Basu (2002). Values of vorticity magnitude, concentration, Mach number, pressure and density along all pathlines were stored. The origins of pathlines were uniformly distributed at a subset of grid points lying outside the mixing layer in both streams.

After initial transients, and before the domain becomes too small, there is a useful interval of self-similar evolution when the mixing layer growth rate is roughly constant. All analyses are over this self-similar stage ($t > t_B$). The Reynolds number Re_ω exceeds 10000 in all cases and flows can be considered to be above the mixing transition. For the inert cases, Re_ω takes on values in the ranges 11540–13410, 15370–18014 and 18586–22353 at $Ma_c = 0.15$, 0.7 and 1.1, respectively; corresponding ranges for the reacting flow cases were 23810–32450, 22150–33970 and 20750–37780. During the initial evolution at the lower Mach number, spanwise vortices undergo pairing, but later there is merely a continuous coalescence into a single large spanwise roller. At the higher Mach number, the mixing layer has little 2-dimensional organization until the eventual formation of the single roller. The growth rate of the mixing layer visual thickness $\delta_{\rm vis}$ (width of the mean vorticity profile between threshold levels) reduces with increasing compressibility or heat release (Figure 2).

Structural changes due to compressibility and heat release may be observed in contour plots of scalar fields.

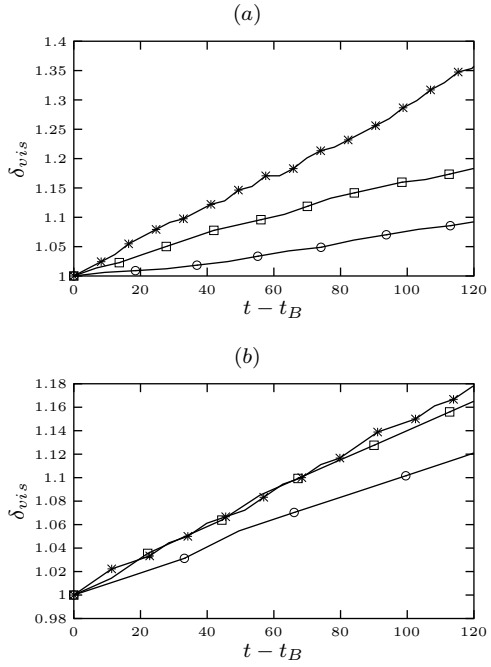

Figure 2: Visual thickness computed $\delta_{\rm vis}$ normalized by the visual thickness at the beginning of the self-similar state, $\delta_{\rm vis,B}$. (a): inert flows; (b): reacting flows. $*$: $M_c = 0.15$, $\square$: $M_c = 0.7$, $\circ$: $M_c = 1.1$

Figure 3 shows oxygen mass fraction and mixture fraction distributions at some instants during the self-similar stage of each simulation. The superposed dark curves are contours used to indicate the mixing layer boundaries. By comparing Figs. 3(a) and 3(c), we may conclude that these boundaries are smoother when compressibility increases. Such changes are quite pronounced with heat release. Even in the essentially incompressible flows at $Ma_c = 0.15$, the mixing layer boundaries are much smoother with heat release (compare Figs. 3(a) and 3(d)). For the reacting flow considered, the stoichiometric mixture fraction value is 0.3. So the heat release takes place closer to the upper boundary (mixture fraction $Z = 0.1$) in Fig. 3(d)–3(f). Consequently, the upper boundaries are very clearly smoother than the lower boundaries at all Mach numbers. In both inert and reacting cases, tongues of freestream fluid penetrate deep into the nominal mixing layer region at the lowest Mach number. At higher compressibility levels the depth of such penetration is much less.

ANALYSES AND RESULTS

A widely prevailing view of the process of entrainment is that large packets of surrounding irrotational fluid are drawn deep into the turbulent region by the action of large scale coherent structures present in the turbulent region. Since the breakdown of these packets and the growth of vorticity should take an $O(1)$ large scale time, engulfed fluid should be present at all times within the turbulent region. To measure the volume of engulfed fluid a criterion must be defined to distinguish between ambient fluid and turbulent fluid. Here we use the lowest reliable thresholds on vorticity magnitude to define essentially irrotational regions, and highest or lowest thresholds on concentrations, which are characteristic of fluids in the streams outside the mixing layer. We consider a lower and upper threshold on vorticity magnitude as 10%

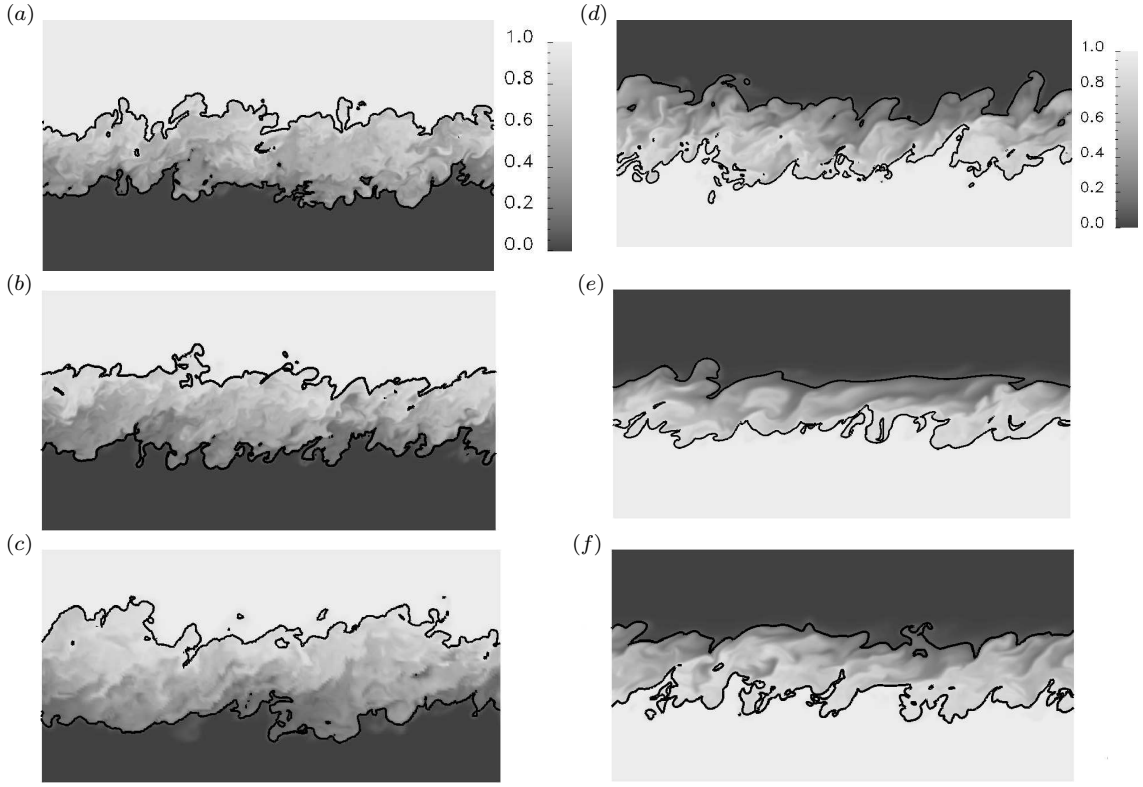

Figure 3: Distributions of oxygen mass fraction from inert flow simulations ((*a*)-(*c*)) and mixture fraction from reacting flows ((*d*)-(*f*)) in an (x, z)-plane at $y/L_y = 0.5$. Black curves are contours at 0.1 and 0.9. (*a*), (*d*)): $Ma_c = 0.15$; (*b*), (*e*)): $Ma_c = 0.7$; (*c*), (*f*)): $Ma_c = 1.1$.

and 20% of $\overline{\omega}_{max}(t)$ which is the maximum of the vorticity, averaged over the homogeneous x and y coordinates at a given time. Similarly thresholds of 0.9 and 0.95 (also 0.05 and 0.1) on the oxygen concentration of the upper and lower streams were used. The choice of thresholds is discussed in detail in Mathew & Basu (2002). With these thresholds, the boundary of the mixing layer was determined from the locations where a threshold was crossed as one approached from the undisturbed parts of the streams. The volume of fluid within this boundary is labelled the volume of mixing layer fluid. Next, all grid points within this boundary where the thresholds were exceeded were found and the associated volumes comprise the mixed fluid volume. The difference between mixing layer volume and mixed fluid volume is the engulfed fluid volume.

Figure 4 shows the growth of mixing layer and engulfed fluid volumes. As expected, growth rate falls with increasing compressibility in both inert and reacting flows. The change is less for the reacting flows. In every case, engulfed volumes and their growth rates are significantly smaller than those of the mixing layer in agreement with DNS (Mathew & Basu 2002) and measurements (Westerweel et al. 2005) of round jets. So engulfment is not a significant process in all these cases.

We turn now to the changes in quantities along pathlines as ambient fluid packets enter and become a part of the turbulent mixing layer. Displacement and elapsed time statistics are listed in Table 2. A relevant local length scale δ_{vis} is the visual thickness; a time scale is $\tau_{vis} = \delta_{vis}/\Delta u$. Only particles which were outside the mixing layer at the beginning of the self-similar evolution stage, and which had entered the mixing layer are taken. All particles that cross the lower threshold do not reach the upper threshold during

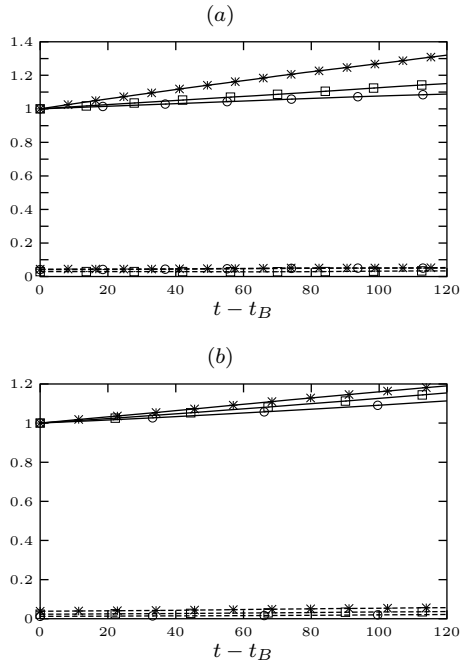

Figure 4: Growth of mixing layer (solid curves) and engulfed fluid volume (dashed) based on concentration thresholds, and normalized with mixing layer volumes at $t = t_B$. (*a*): inert flows; (*b*): reacting flows. Symbols as in Fig. 2

the interval considered. Subscript 0 denotes the initial position, l and u denote lower and upper thresholds, respectively, ω denotes use of vorticity thresholds while C stands for either mass (Y) or mixture (Z) fraction. It is evident that in every case, the displacements Δz from the original location to the point where even the upper thresholds are crossed are small compared with the thickness of the mixing layer. The mean displacement is less than 10% of the mixing layer thickness in all cases, and even maximum displacements are only around half the mixing layer width. In Mathew & Basu (2002), the elapsed time between thresholds were also small, about 30% of the local O(1) time. Here, growth of vorticity in the inert, incompressible layer is the fastest at 0.46. Compressibility increases the elapsed time, and heat release has a more pronounced effect—in fact, it takes an O(1) duration for vorticity to increase from the lower to the upper threshold. The growth of the scalar is slower than that of vorticity, as expected because the flow is organized by the vorticity field, and takes and O(1) time when either compressiblilty effects or heat release is present. The low speed results are in agreement with the previous finding in the incompressible round jet.

The effect of compressibility and heat release acting independently or together is to delay entrainment (growth of vorticity) and mixing (molecular level scalar transport). We understand this as fluid particles being convected downstream near the edges of the mixing layer while acquiring vorticity, with little displacement across the layer. Scalar transport is delayed further as the mixing layer boundaries become smoother and the area available for the small-scale diffusive transport is reduced.

The pdf of Mach number at the point on fluid pathlines when the lower threshold is crossed provides another facet of the entrainment process and the changes with compressibility and heat release. The pdfs for all cases are shown in Fig. 5. In the essentially incompressible flows (inert or reacting), the pdf rises sharply close to the convective Mach number and falls even more sharply thereafter: most of the fluid packets are travelling at roughly the freestream speed when they enter the mixing layer. With increasing compressibility, the pdf broadens considerably; the peak is close to the convective Mach number. With heat release the pdf is broadened further. Now, the Mach number of many more fluid packets have become lower before they have become a part of the turbulent mixing layer.

SUMMARY AND CONCLUSIONS

The study has shown that the volume and growth rate of engulfed fluid remain small in plane mixing layers also, even though the layer can exhibit large scale organization. Also, as seen before in round jets, entrainment occurs close to the turbulent-nonturbulent boundaries. Neither compressibility nor heat release, which causes easily observable structural changes and reduces layer growth rate, alters these characteristics. However, both retard the entrainment process considerably. The evidence is more compelling because the Reynolds numbers are well above the mixing transition.

ACKNOWLEDGMENTS

This work was initiated during Inga Mahle's stay in IISc on a DAAD fellowship. She gratefully acknowledges DAAD, and IISc for the hospitality. She also thanks FORTVER, the Bavarian Competence Center for Turbulent Combustion for financial support.

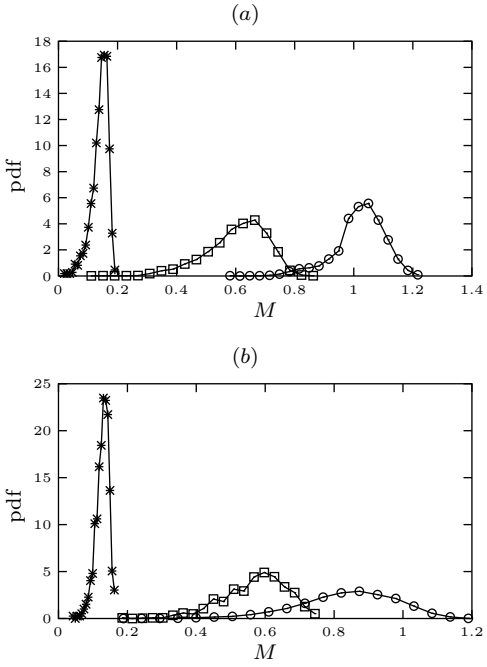

Figure 5: Pdfs of the local Mach number magnitude at the time when the particles are crossing the upper vorticity threshold. (a): Inert flows; (b) reacting flows. Symbols as in Fig. 2

REFERENCES

Brown, G. L., and Roshko, A., 1974, "On density effects and large structure in turbulent mixing layers", *J. Fluid Mech.* Vol 64, pp. 775–816.

Corrsin, S., Kistler, A. L., 1955, "Free-stream boundaries of turbulent flows", *NACA Tech Rep. No. 1244.*

Papamoschou, D., Roshko, A., 1988, "The compressible turbulent shear layer: an experimental study", *J. Fluid Mech.* Vol. 197, pp. 453-477.

Mahle, I., 2007, "Direct and large-eddy simulation of inert and reacting compressible turbulent shear layers", Dr. Ing. thesis, Technische Universität München (*under preparation*).

Mathew, J., Basu, A.J., 2002, "Some characteristics of entrainment at a cylindrical turbulence boundary", *Phys. Fluids* Vol. 14(7), pp. 2065-2072.

Sesterhenn, J., 2000, "A characteristic-type formulation of the Navier-Stokes equations for high order upwind schemes", *Computers & Fluids* Vol. 30, pp. 37-67.

Westerweel, J., Fukushima, C., Pedersen, J.M., Hunt, J.C.R., 2005, "Mechanics of the Turbulent-Nonturbulent Interface of a Jet", *Phys. Rev. Lett* 95, 174501.

Table 2: Statistics of displacements and elapsed times for growth of vorticity and mass fraction or mixture fraction along pathlines. N is the sample size. z_0 is the initial z-coordinate of a pathline. Subscript C stands for mass fraction Y for inert flows and mixture fraction Z for reacting flows.

M_c	Quantity	N	Inert			N	Reacting		
			Mean	Max	Min		Mean	Max	Min
0.15	$\lvert z_0 - z_{\omega l}\rvert / \delta_{vis}\,(t_l)$	5107	0.0829	0.5117	0	2952	0.0828	0.3233	0
	$\lvert z_0 - z_{\omega u}\rvert / \delta_{vis}\,(t_l)$	4220	0.0971	0.6001	0	2229	0.0891	0.5410	0
	$\lvert z_{\omega u} - z_{\omega l}\rvert / \delta_{vis}\,(t_l)$	4220	0.0250	0.5201	0	2229	0.0188	0.5410	0
	$\lvert z_0 - z_{Cl}\rvert / \delta_{vis}\,(t_l)$	5010	0.0833	0.5224	0	1654	0.0870	0.3668	0
	$\lvert z_0 - z_{Cu}\rvert / \delta_{vis}\,(t_l)$	3875	0.1044	0.5920	0	859	0.0997	0.5991	0
	$\lvert z_{Cu} - z_{Cl}\rvert / \delta_{vis}\,(t_l)$	3875	0.0337	0.5878	0	859	0.0398	0.5766	0
	$(t_{\omega u} - t_{\omega l}) / t_{vis}$	4220	0.4696	9.1722	0	2229	0.6437	9.6366	0
	$(t_{Cu} - t_{Cl}) / t_{vis}$	3875	0.6144	8.6643	0	859	0.9912	11.5919	0
	$(t_{Cl} - t_{\omega l}) / t_{vis}$	4728	0.0301	5.4441	-5.8458	1646	0.9502	6.2618	-5.7861
	$(t_{Cu} - t_{\omega u}) / t_{vis}$	3636	0.1419	6.3473	-9.1722	853	1.2797	11.3474	-9.6366
0.7	$\lvert z_{\omega u} - z_{\omega l}\rvert / \delta_{vis}\,(t_l)$	13959	0.0290	0.6667	0	5098	0.0253	0.8277	0
	$\lvert z_0 - z_{\omega l}\rvert / \delta_{vis}\,(t_l)$	12760	0.0741	0.4947	0	4288	0.0794	0.3203	0
	$\lvert z_0 - z_{\omega u}\rvert / \delta_{vis}\,(t_l)$	12760	0.0930	0.7481	0	4288	0.0889	0.8215	0
	$\lvert z_{Cu} - z_{Cl}\rvert / \delta_{vis}\,(t_l)$	13608	0.0423	0.6769	0	3738	0.0513	0.8277	0
	$\lvert z_0 - z_{Cl}\rvert / \delta_{vis}\,(t_l)$	11792	0.0796	0.4947	0	2482	0.0807	0.4233	0
	$\lvert z_0 - z_{Cu}\rvert / \delta_{vis}\,(t_l)$	11792	0.1084	0.7481	0	2482	0.1063	1.0385	0
	$(t_{\omega u} - t_{\omega l}) / t_{vis}$	12760	0.8359	17.8751	0	4288	1.1730	25.8824	0
	$(t_{Cu} - t_{Cl}) / t_{vis}$	11792	1.1986	19.4045	0	2482	1.8754	26.5387	0
	$(t_{Cl} - t_{\omega l}) / t_{vis}$	13333	0.3018	9.8935	-13.2233	3721	1.1978	13.9185	-14.2523
	$(t_{Cu} - t_{\omega u}) / t_{vis}$	11561	0.6607	17.7959	-17.7959	2466	1.7592	26.5387	-22.5871
1.1	$\lvert z_{\omega u} - z_{\omega l}\rvert / \delta_{vis}\,(t_l)$	6962	0.0205	0.3878	0	7009	0.0224	0.5050	0
	$\lvert z_0 - z_{\omega l}\rvert / \delta_{vis}\,(t_l)$	5364	0.0558	0.3641	0	6265	0.0943	0.3278	0
	$\lvert z_0 - z_{\omega u}\rvert / \delta_{vis}\,(t_l)$	5364	0.0698	0.3801	0	6265	0.0960	0.5879	0
	$\lvert z_{Cu} - z_{Cl}\rvert / \delta_{vis}\,(t_l)$	5441	0.0362	0.5031	0	5528	0.0045	0.6849	0
	$\lvert z_0 - z_{Cl}\rvert / \delta_{vis}\,(t_l)$	2909	0.0633	0.3641	0	4134	0.0911	0.3713	0
	$\lvert z_0 - z_{Cu}\rvert / \delta_{vis}\,(t_l)$	2909	0.0936	0.5031	0	4134	0.0999	0.6849	0
	$(t_{\omega u} - t_{\omega l}) / t_{vis}$	5364	0.7808	9.8476	0	6265	1.0353	34.9646	0
	$(t_{Cu} - t_{Cl}) / t_{vis}$	2909	1.2193	9.8476	0	4134	1.6721	47.8477	0
	$(t_{Cl} - t_{\omega l}) / t_{vis}$	5299	0.5850	7.9822	-8.2881	5517	1.4929	18.1162	-20.5031
	$(t_{Cu} - t_{\omega u}) / t_{vis}$	2841	0.9067	9.8476	-9.4413	4131	2.1170	35.8840	-24.8244